International Journal of
INTELLIGENT SYSTEMS AND APPLICATIONS IN ENGINEERING
ISSN:2147-6799 www.ijisae.org Original Research Paper

# Heart Disease Detection from Neonatal Infrared Thermograms Using Multiresolution Features and Data Augmentation

**Duygu Savasci*[1], Murat Ceylan[2], Ahmet Haydar Ornek[3], Murat Konak[4], Hanifi Soylu[5]**

**Submitted: 21/01/2020 Accepted: 02/03/2020**

***Abstract:*** Monitoring temperature changes of infants in the neonatal intensive care unit is very important. Especially for premature and very low birthweight infants, determining temperature changes in their skin immediately is extremely significant for follow-up processes. The development of medical infrared thermal imaging technologies provides accurate and contact-free measurement of body temperature. This method is used to detect thermal radiation emitted from the body to obtain skin temperature distributions. The purpose of this study is to develop an analysis system based on infrared thermal imaging to classify neonates who are healthy and suffering from heart disease using their skin temperature distribution. In this study, 258 infrared thermograms obtained applying data augmentation on 43 infrared thermograms captured from the Neonatal Intensive Care Unit were used. The following operations were performed: firstly, images were segmented to eliminate unnecessary details on the thermogram. Secondly, the features of the image were extracted applying Discrete Wavelet Transform (DWT), Ridgelet Transform (RT), Curvelet Transform (CuT), and Contourlet Transform (CoT) which are multiresolution analysis methods. Finally, these features are classified as healthy and unhealthy using classification methods such as Artificial Neural Network (ANN), Support Vector Machine (SVM) and Random Forest (RF). The best results were obtained with SVM as 96.12% of an accuracy, 94.05% of a sensitivity and 98.28% of a specificity.

***Keywords:*** Artificial Neural Network, Data Augmentation, Infrared Thermal Imaging, Neonate, Multiresolution Analysis Methods, Random Forest, Support Vector Machine.

## 1. Introduction

All objects having above absolute zero (0K, -273,15℃) emit infrared radiation, depending on their temperature [1]. The amount of radiation emitted by the body is in the infrared area of the electromagnetic spectrum and the wavelength is in the range of 0.75-1000 micrometers [2]. Infrared cameras convert the emitted infrared radiation into electronic signals. These signals are matched to colors and then they are displayed on the screen [3]. The visual display of this temperature distribution is called a thermogram. The thermogram displayed as pixels arranged in a two-dimensional array. Each pixel represents the temperature values of the displayed region [4].

Medical infrared thermal imaging is an imaging technique which can determine the temperature distribution of organs and tissues by capturing infrared radiation. Thermal imaging can be used as a diagnostic tool on a variety of conditions to advise treatment, evaluate the effects of treatment and examine physiological functions in body [2]. Recently, due to the rapid development of medical thermal imaging technologies, medical imaging has become a very important imaging technique for continuous monitoring of infants in neonatal intensive care. Thermal imaging is a non-invasive, un-ionized, non-contact, fast, simple and harmless method that can detect temperature changes caused by physiological dysfunctions in the body of neonatal. Physiological dysfunctions in the body such as inflammation and infection cause temperature increases. These increases are shown as hot spots or asymmetric patterns in thermal images. The skin temperature distribution of a healthy human body shows contralateral symmetry. On the other hand, the temperature distribution which is above a certain level indicates strong abnormalities [5]. Therefore, it is possible to monitor the thermal asymmetry or thermal differences depending on time in the pre-diagnosis of diseases or in the evaluation of follow-up treatment. The detection of anomalies by the aid of the asymmetries observed at body temperature distribution revealed the idea of pre-diagnosing system installation by using thermograms. Thus, the purpose of the presented this study is to build a pre-diagnosis system based on non-contact, non-invasive, and un-ionizing infrared thermal imaging.

The organization of this study is as follows. In section 2, we present used data, segmentation, multiresolution analysis methods, artificial neural network, support vector machine, random forest and evaluation of classification results. Section 3 describes the experiments and results. Section 4 discusses the obtained results. Finally, conclusions and perspectives of future work are given in the last section.

## 2. Material and Methods

In this study, firstly, the thermograms were captured by the thermal camera. Secondly, thermograms were segmented to eliminate unnecessary details. Thirdly, the features of the image were extracted by using Multiresolution Analysis methods.

[1] *Konya Technical University, Electrical-Electronic Engineering Dept., Konya, Turkey; ORCID ID: 0000-0002-4495-9040*
[2] *Konya Technical University, Electrical-Electronic Engineering Dept., Konya, Turkey; ORCID ID: 0000-0001-6503-9668*
[3] *Konya Technical University, Electrical-Electronic Engineering Dept., Konya, Turkey; ORCID: 0000-0001-7254-9316*
[4], *Selcuk University, Faculty of Medicine, Department of Pediatrics, Konya, Turkey; ORCID ID: 0000-0001-8728-4541*
[5] *Selcuk University, Faculty of Medicine, Department of Pediatrics, Konya, Turkey; ORCID ID: 0000-0003-0367-859X*
* *Corresponding Author Email: duyguzn8559@gmail.com*

Fourthly, these features were given to Artificial Neural Network, Support Vector Machine and Random Forest as inputs and the thermograms were classified as unhealthy or healthy. Finally, results of the classification methods were compared in terms of their accuracy, sensitivity and specificity rates.

### 2.1. Used Data

The thermograms of neonates were captured from the Neonatal Intensive Care Unit that is in the Faculty of Medicine of Selcuk University. The VarioCAM HD infrared camera of InfraTec, which operates in the long wavelength range, was used to record thermograms. This camera has a 640x480 resolution and its thermal sensitivity is about 0.05°C. The infrared camera was placed about 60-100 cm away from the neonatal who was in the supine position. Thermograms captured by infrared camera were transferred to a computer. Thermogram acquisition procedure is shown in Fig. 1 [6]. Thermograms were obtained from neonates ranging between 23-42 weeks of gestational age in the neonatal intensive care between April 2017 and March 2018.

**Fig. 1.** Thermogram acquisition procedure [6].

The thermograms can be converted to either raw RGB or a raw temperature map using a portable computer and thermal camera software. In this study, thermograms were converted to RGB. The color range of the RGB images is determined based on the lower and upper threshold temperature values entered by using the thermal camera software [7]. Fig. 2 shows thermograms produced by using a lower threshold value of 30 °C and an upper threshold value of 40 °C.

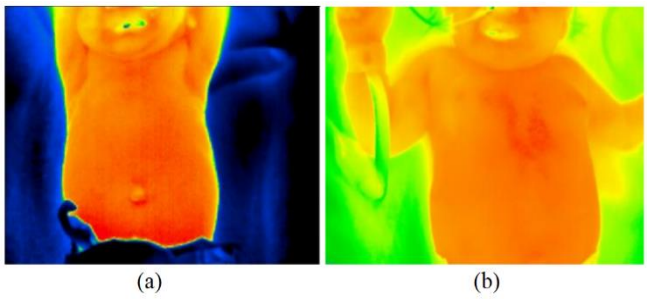


**Fig. 2.** Thermograms belonging to (a) healthy (b) unhealthy neonates

### 2.2. Segmentation

A segmentation operation was carried out on thermograms to extract the background (outside of the neonatal body) of the image. We used the Graph Cut which is in the Image Segmenter app of MATLAB to segment an image. The Graph Cut is a semiautomatic segmentation technique which can be used to segment an image into foreground and background elements. Segmentation operation with Graph Cut is performed by drawing lines which are called scribbles on the image to identify what you want in the background and what you want in the foreground. The Image Segmenter segments the image automatically based on your scribbles and displays the segmented image. After the segmentation operation, RGB images were converted to gray-level images for the purpose of standardization. Fig. 3b illustrated segmented gray-level thermogram produced from RGB thermogram in Fig. 3a.

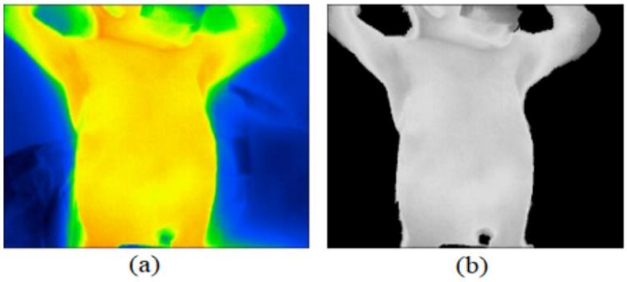


**Fig. 3.** (a) RGB thermogram (b) Gray level and segmented thermogram.

### 2.3. Multiresolution Analysis Methods (MRA)

#### 2.3.1. Wavelet Transform (WT)

Multiresolution analyses are based on WT. The WT extracts features of the image by performing shifting or scaling operations [8]. In Discrete Wavelet transform (DWT), the scale and shift parameters are represented in a discrete time-scale domain. DWT can be implemented as a set of filter banks, comprising high- pass and low-pass filters [9]. For images, two-dimensional (2D) DWT is achieved by applying the 1D-DWT to the rows and columns of the image separately. DWT decomposes the image into the approximation coefficient (LL) which is the low-frequency component and the detail coefficients (LH, HL, HH) which are the high-frequency components. Multi-level decomposition can be performed by decomposing the approximation component multiple times in the same way [10]. One level analysis filter bank for 2D-DWT can be seen in Fig. 4.

#### 2.3.2. Ridgelet Transform (RT)

Wavelet transform produces good performance for piecewise smooth functions in one dimension, however, it does not perform well in the two-dimensional case. To overcome this weakness of Wavelets, Ridgelet Transform which deals effectively with line singularities in 2D was introduced. RT is based on the Radon transform [11].

RT can be achieved in the Fourier domain (Fig. 5). Firstly, 2D Fast Fourier transform (FFT) is applied. Then, Fourier coefficients are interpolated along lines which pass through the frequency space and 1D inverse FFT is calculated. After that, the Radon Transform is used to map a line singularity into a point singularity. Finally, 1D WT is applied to handle the point singularity in the Radon domain. As a result, RT coefficients matrix of the image is obtained [12].

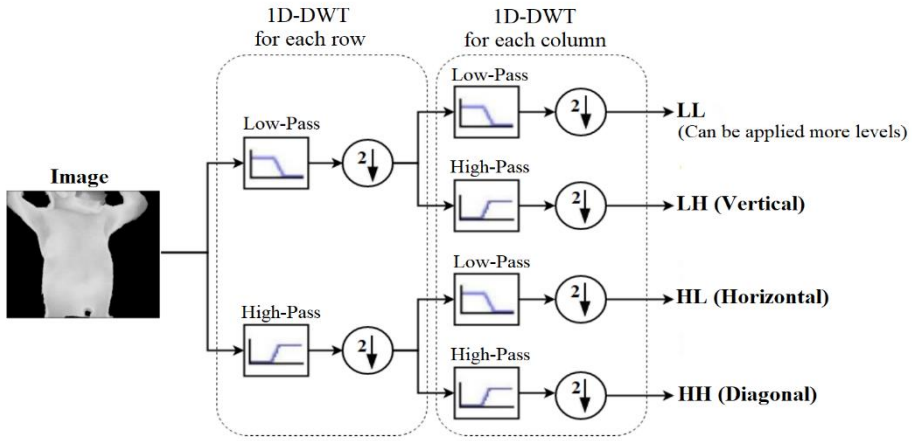


**Fig. 4.** One level analysis filter bank for 2D-DWT [10].

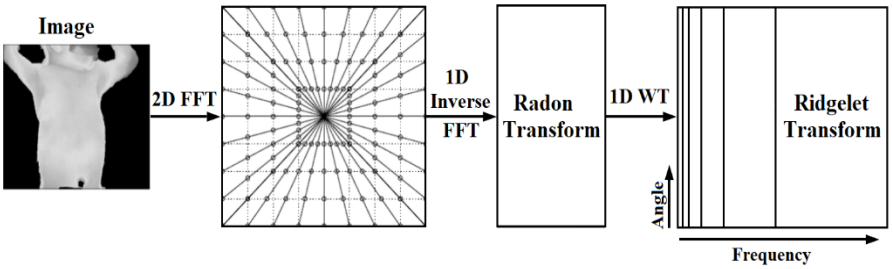


**Fig. 5.** Ridgelet transform flowchart [12].

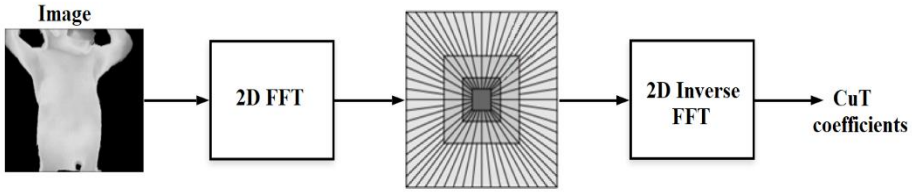


**Fig. 6.** Fast Discrete Curvelet Transform scheme [14].

### 2.3.3. Curvelet Transform (CuT)

The CuT produces better accuracy representing the edges and other singularities along curves in the image. A new design of CuT, i.e., Fast Discrete Curvelet Transform (FDCT), was introduced in 2006. This transform is faster, simpler, and easier to understand than First-Generation CuT. The FDCT is a multiscale and multidirectional transform that provides a better representation of the objects with edges. The FDCT can be implemented via either the Unequally Spaced Fast Fourier Transform (USFFT) or the Wrapping method. These transforms give different features at different angles at a given scale [13]. The curvelets via Wrapping method are described in four basic steps:

**Step 1:** Compute 2D FFT coefficients to obtain Fourier samples $\hat{f}[n_1, n_2]$

**Step 2:** Interpolation is applied for each scale (j) and angle ($l$) pair and form the product $\tilde{u}_{j,l}[n_1, n_2]\ \hat{f}[n_1, n_2]$

**Step 3:** Wrap result of step 2 around the origin and obtain $\hat{f}_{j,l}[n_1, n_2] = W(\tilde{u}_{j,l}\hat{f})[n_1, n_2]$, where the range for $n_1$ and $n_2$ are $0 \leq n_1 < L_{1,j}$ and $0 \leq n_2 < L_{2,j}$ (for $\theta$ in the range $(-\pi/4, \pi/4)$)

**Step 4:** Implement the inverse 2D FFT for each $\hat{f}_{j,l}$ to obtain the curvelet coefficients [13].

A scheme of the FDCT is shown in Fig. 6 [14]. Firstly, a 2D Fast Fourier Transform (FFT) is applied to an image. After that, the 2D Fourier frequency plane is split into wedges. The wedges have a parabolic shape as the Fourier plane is divided into radial and angular partitions. Finally, 2D inverse FFT is applied to each wedge to find the curvelet coefficients.

### 2.3.4. Contourlet Transform (CoT)

The CoT offers a flexible multiresolution and directional decomposition for images as it allows for a different number of directions at each scale [15]. This transform improves the contours or provides a smooth representation of such contours using fewer coefficients than those required by Wavelets [16].

CoT is formed of two major elements, which are the Laplace Pyramid (LP) and Directional Filter Bank (DFB). LP is used to capture the point discontinuities. The LP produces approaches such as low-pass filtering and down-sampled for the signal. Then, DFB is used to link these point discontinuities into linear structures [17]. A filter bank structure of the Contourlet for images is shown in Fig. 7.

## 2.4. Artificial Neural Network (ANN)

ANN is one of the most popular methods of machine learning methods and is widely in situations which are nonlinear, multidimensional, complex, and uncertain, and in which the relationship between variables is unknown [18].

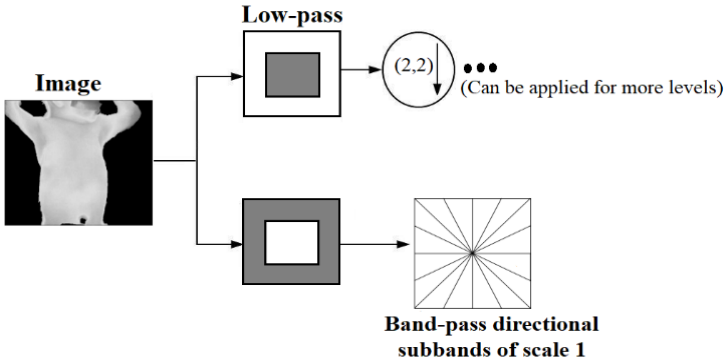


**Fig. 7.** Contourlet filter bank structure.

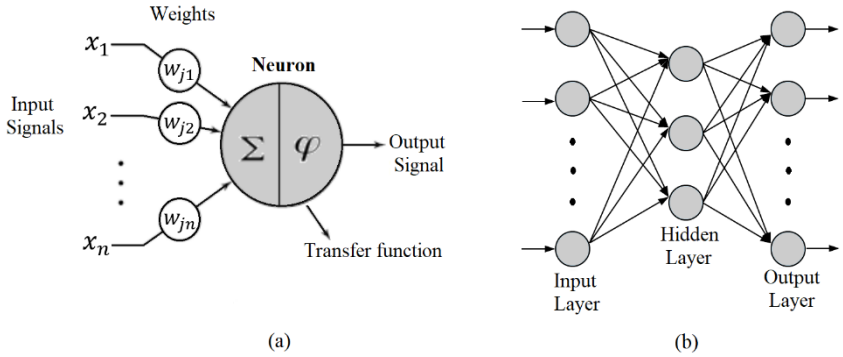


**Fig. 8. (**a) The basic function of elements of neuron (b) Structure of a typical neural network.

An ANN is a network consisting of basic processing units (named nodes or neurons) which can operate in parallel. These units are the mathematical model of neurons in the human brain in the computer environment [19]. The basic function of elements of a neuron is illustrated in Fig. 8a. The neurons in the neural network are connected by links and each link has a numerical weight associated with it. Each neuron receives input signals through its connections and is multiplied by a numerical weight. At each neuron, the weighted input signals are summed and then this combined input is passed through a transfer function to produce the output of the neuron [20]. This operation can be optimized for different problems by setting the neuron numbers in layers and having various parameters which are specific to ANN.

The ANN structures typically consist of three layers: an input layer, a hidden layer, and an output layer (Fig. 8b). These layers can be structured hierarchically [20]. The network alters its weight parameters throughout the set of training data and tries to learn until it can find a set of weights that will produce the smallest possible error for input-output mapping [21].

### 2.5. Support Vector Machine (SVM)

SVM is a binary classification method that attempts to establish a decision boundary between the input data of any two classes. Input data are transformed to high-dimensional feature space through use of nonlinear kernel functions, so that the transformed data becomes more separable compared to the original input data. In this feature space a linear decision surface is constructed with special properties that ensure high generalization ability of the learning machine [22]. SVM creates a hyperplane or a set of hyperplanes in a high-dimensional feature space that can be used for classification, as shown in Fig. 9.

There are many possible hyperplanes (Fig. 9a) that could be chosen to separate the two classes of data points. Among the separating hyperplanes, the one for which the distance to the closest point is maximal is called optimal separating hyperplane [23]. An optimal hyperplane is defined as the linear decision function with maximal margin between the data points of the two classes (Fig. 9b). The support vectors define the margin of largest separation between the two classes [22]. Support vectors are data points that are closer to the hyperplane.

SVM can perform a linear and nonlinear classification with kernels such as linear, polynomial, and radial basis function (RBF) [24]. The choice of a kernel function often has a bearing on the results of analysis.

### 2.6. Random Forest (RF)

A RF is a classification algorithm consisting of many individual decision trees that operate as an ensemble. The decision forests are composed of combining individual decision trees [25].

RF grows many classification trees. Once the forest is trained as explained below, to classify a new feature vector from an input vector, it is run across all the trees grown in the forest. Each tree gives classification for the feature vector which is recorded as a vote. The votes from all trees are combined and the class for which maximum votes are counted (majority voting) is declared as classification of the new feature vector.

Each tree is grown in RF as follows:

- N training data are sampled at random with replacement, from the original data. This sample will be the training set for growing the tree.
- If there are M input variables, a number m is selected as less or equal than M such that at each node, m variables are selected at random out of M. This m value is kept constant during forest growing.
- Each tree is grown to the largest extent possible [26]. (There is no pruning or stopping rule during classification [27].

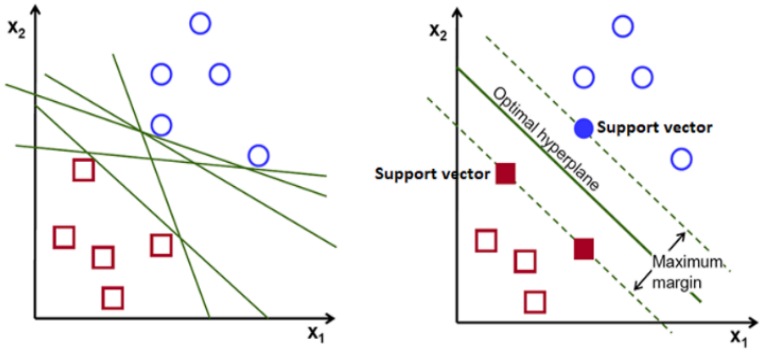


**Fig. 9.** (a) Possible hyperplanes (b) Optimal hyperplane using the SVM.

### 2.7. Evaluation of Classification Results

There are various methods for evaluating classification results. In this study, sensitivity, specificity, and accuracy rates were computed to analyse the results of the thermograms classification. The accuracy, sensitivity, and specificity rates were calculated as seen in Table 1 [28].

True Positives (TP): Classification of an unhealthy labeled subject as unhealthy by ANN.

True Negatives (TN): Classification of a healthy labeled subject as healthy by ANN.

False Positives (FP): Classification of a healthy labeled as unhealthy by ANN.

False Negatives (FN): Classification of an unhealthy labeled as healthy by ANN.

**Table 1.** Calculation of accuracy, sensitivity and specificity rates.

| | |
|---|---|
| Accuracy (%) | $\frac{TP + \mathrm{TN}}{TP + TN + FP + FN} x100$ |
| Sensitivity (%) | $\frac{TP}{TP + FN} x100$ |
| Specificity (%) | $\frac{TN}{TN + FP} x100$ |

## 3. Experiments and Results

In this study, the success rates of the ANN, SVM, and RF classification methods which are used to diagnose heart disease are analysed thoroughly by using thermograms, which were obtained from 14 unhealthy neonates diagnosed with heart trouble (coarctation of the aorta and pulmonary artery) and 29 healthy neonates in the neonatal intensive care unit.

As a result, totally 43 neonates were included to the study. Firstly, segmentation operation was performed on thermograms belonging to 43 neonates. Then, the data augmentation method was used to increase this number of images. The data augmentation method allows us to produce different variations of images. These variations include randomly cropping parts from input images, horizontally rotating of images, and applying affine transformations (rotation, rescaling, translations, etc.) to images. In this study, the data augmentation method was applied to 43 thermograms. As a result, a further five images were produced for each image. Fig. 10 illustrates the images obtained after the data augmentation method was applied. After this operation, the number of images for each neonatal increased to six. Thus, a total of 258 thermograms (174 healthy-labeled and 84 unhealthy-labeled) were used [29]. Then, the thermograms which were of size 362 × 482 were rescaled to a size of 256 × 256 to use in multiresolution analysis.

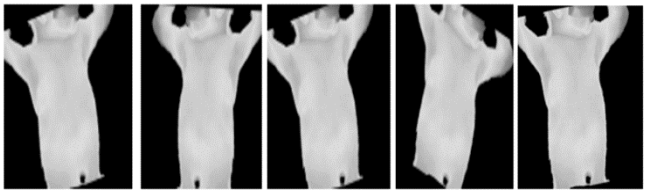

**Fig. 10**. Produced images after the data augmentation method was applied [29].

Secondly, the multiresolution analysis methods (DWT, RT, CuT, and CoT) were used to extract features of thermograms. Thermograms were divided into approximation and detail coefficients by using multiresolution analysis methods. The features of thermograms were extracted from the matrix of approximation coefficients. The approximation coefficient matrix was obtained for each image, separately. The decomposition level was chosen as 3 for DWT, CuT, and CoT transforms and 2 for RT transform, empirically. The obtained matrix of approximation coefficients was transformed into column vectors to generate feature vectors. Then, these feature vectors were normalized in the range [0, 1].

Thirdly, machine learning classification methods such as ANN, SVM, and RF were used to classify thermograms. The feature vectors were given as an input to the ANN, SVM, and RF and a classification process was conducted. Target values of ANN, SVM, and RF for healthy and unhealthy thermograms were 0 and 1, respectively. The 10-fold cross-validation algorithm was applied to verify classification validity. Accuracy, sensitivity and specificity rates were calculated in order to compare the classification results of the ANN, SVM, and RF. The obtained values were presented in Table 2. The best results of each classification method were in bold. These tasks were performed using MATLAB. The proposed system diagram is given in Fig. 11.

The structure belonging to ANN used in the study is three-layered (input layer, a hidden layer, and output layer), feed-forward and back-propagated. The logarithmic sigmoid was used as an activation function for the hidden layer. Gradient descent with momentum was chosen as a training algorithm. If an ANN output for classification was less than 0.5, it was labeled as healthy, if it was equal or greater than 0.5, it was labeled as unhealthy. Optimum ANN parameters were determined empirically. The value of stopping criteria, maximum iteration number,

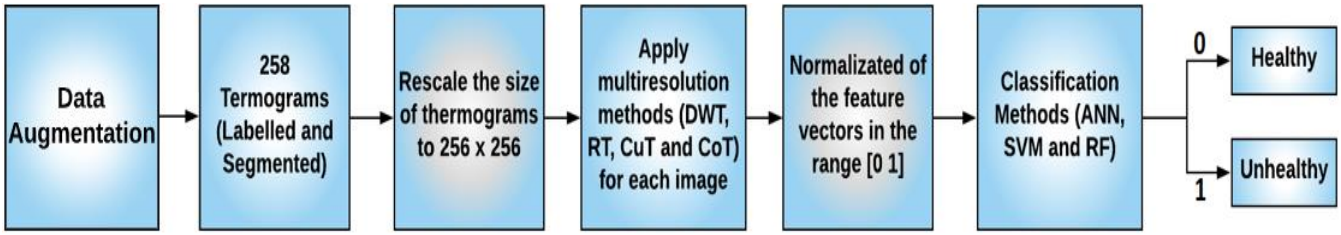


**Fig. 11.** Block representation of the proposed system.

momentum constant, and the number of nodes in the hidden layer were as 1e-20, 300, 0.2, and 50, respectively. The learning parameter was as 0.6 for DWT, 0.02 for RT, 0,6 for CuT and 1 for CoT.

The most optimal method in the SVM which yields high classification success was determined by evaluating three kernel functions such as Linear, Polynomial, and Radial Basis. After these functions were compared based on their classification results, the polynomial kernel function was selected as the most optimal method.

The number of trees for RF is one of the factors that affects correctness of classification significantly. The optimal number of decision trees which forms decision forest were sought empirically. In this empirical study, the following number of trees were evaluated: 10, 30, 100, and 1000. The optimal number of trees was determined as 100 based on processing time and accuracy rate of classification. In addition, it was observed that as number of trees increases, processing time increases.

According to Table 2, the best method for classifying the 258 thermograms is the SVM. Among the classification methods, the highest sensitivity rate was obtained by SVM with 94.05%, which indicates the success of SVM classifier in diagnosing the disease. The specificity rate for SVM and RF classification methods are almost the same. High specificity rate found 97-98% is a strong indicator of success of classifier in detecting healthy neonates.

Performance of MRA methods (DWT, RT, CuT, and CoT) of each classification methods was compared. The accuracy of all MRA methods is over 90%. According to accuracy results, DWT and CoT are the most efficient MRA methods for classification. The highest accuracy for ANN is obtained using CuT and CoT, whereas using RT generates the highest accuracy rate for RF.

Table 3 shows the confusion matrices obtained according to the results of the classification methods of 258 thermograms. As can be seen in Table 3, among the classification methods, 171 of 174 healthy-labeled images were classified as a healthy using SVM with DWT, whereas 79 of 84 unhealthy-labeled images were classified as an unhealthy using SVM with CoT.

**Table 2**. Classification results of 258 thermograms.

| Classification Methods | MRA Methods | Accuracy (%) | Sensitivity (%) | Specificity (%) |
|---|---|---|---|---|
| **ANN** | DWT | 90.7 | **86.91** | 92.53 |
| | RT | 90.7 | 84.52 | 93.68 |
| | CuT | **91.09** | 84.52 | **94.25** |
| | CoT | **91.09** | 85.71 | 93.68 |
| **SVM** | DWT | **96.12** | 91.67 | **98.28** |
| | RT | 94.58 | 89.29 | 97.13 |
| | CuT | 95.35 | 90.48 | 97.70 |
| | CoT | **96.12** | **94.05** | 97.13 |
| **RF** | DWT | 90.7 | 77.38 | **97.13** |
| | RT | **93.41** | **85.71** | **97.13** |
| | CuT | 91.47 | 80.95 | 96.55 |
| | CoT | 91.09 | 78.57 | **97.13** |

## 4. Discussion

The methods (ANN, SVM, and RF) classifying 43 thermograms, and 258 thermograms generated using data augmentation were compared in terms of accuracy, sensitivity, and specificity rates. The results are presented in Fig. 12, Fig. 13, and Fig. 14. Whereas ANN-1, SVM-1 and RF-1 show the classification methods which used 43 thermograms, ANN-2, SVM-2 and RF-2 depict the classification methods that used 258 thermograms obtained by applying data augmentation method. According to the results, data augmentation method that was used to increase the number of images affected the classification results positively.

**Table 3.** Confusion matrices for classification results.

| MRA Methods | | ANN Confusion Matrix | | SVM Confusion Matrix | | RF Confusion Matrix | |
|---|---|---|---|---|---|---|---|
| | | Unhealthy (predicted) | Healthy (predicted) | Unhealthy (predicted) | Healthy (predicted) | Unhealthy (predicted) | Healthy (predicted) |
| **DWT** | **Unhealthy (actual)** | 73 | 11 | 77 | 7 | 65 | 19 |
| | **Healthy (actual)** | 13 | 161 | 3 | 171 | 5 | 169 |
| **RT** | **Unhealthy (actual)** | 71 | 13 | 75 | 9 | 72 | 12 |
| | **Healthy (actual)** | 11 | 163 | 5 | 169 | 5 | 169 |
| **CuT** | **Unhealthy (actual)** | 71 | 13 | 76 | 8 | 66 | 18 |
| | **Healthy (actual)** | 10 | 164 | 4 | 170 | 6 | 168 |
| **CoT** | **Unhealthy (actual)** | 72 | 12 | 79 | 5 | 66 | 18 |
| | **Healthy (actual)** | 11 | 163 | 5 | 169 | 5 | 169 |

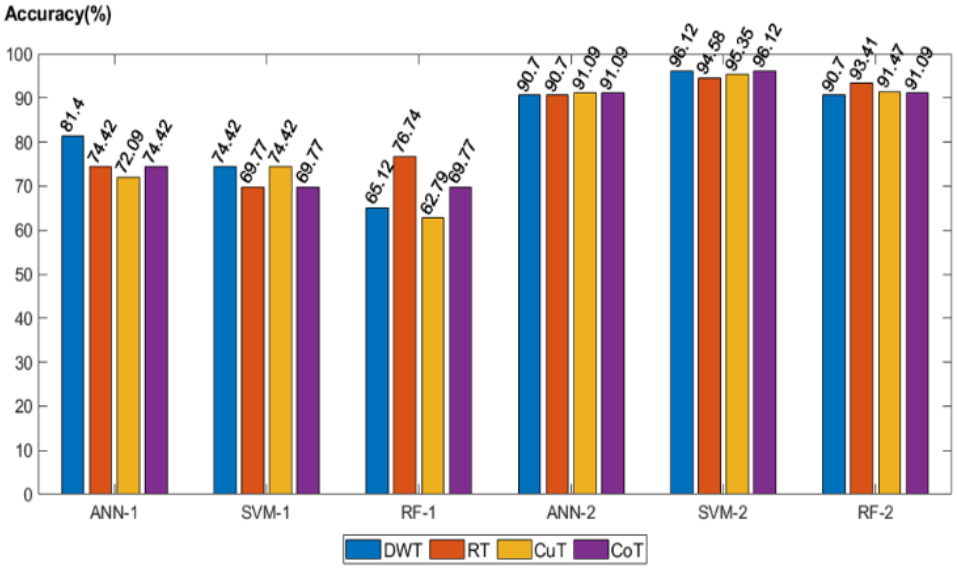


**Fig. 12.** Accuracy rates for 43 thermograms and 258 thermograms.

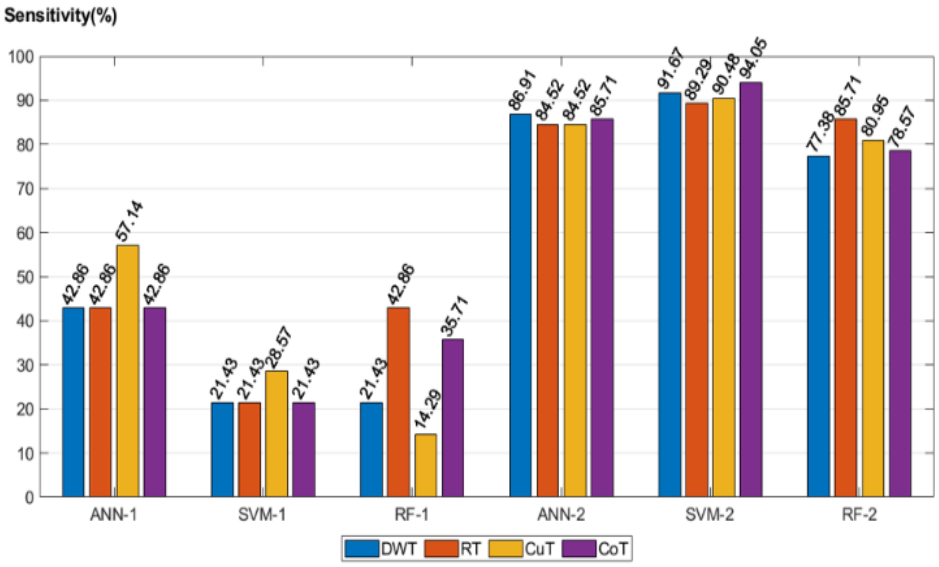


**Fig. 13.** Sensitivity rates for 43 thermograms and 258 thermograms.

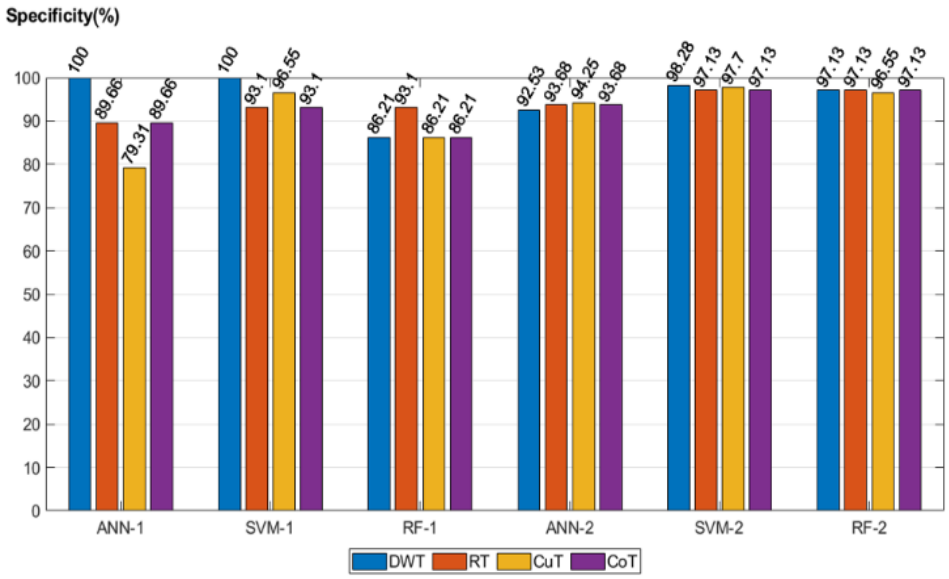


**Fig. 14.** Specificity rates for 43 thermograms and 258 thermograms.

In Fig. 12, the highest accuracy rate of the classification of 43 thermograms is 81.4%, whereas the accuracy rate increased to 96.12% in the classification of 258 thermograms obtained using the data augmentation method. It is explicit that using 258 thermograms obtained applying data augmentation method significantly increased accuracy and sensitivity rates. SVM classifier produced the highest accuracy rate in the classification.

In Fig. 13, although the highest sensitivity rate was 57.14% for the classification of 43 thermograms, this rate dramatically rose to 94.05% for the classification of 258 thermograms. It is clear that difference of two sensitivity rates is huge (36.91%). This difference shows how data augmentation affected classification result significantly. High sensitivity rate found between 89% and 94% show the positive effect of data augmentation method on classification. Based on these results, it can easily be said that using 43 thermograms in classification did not end up with high classification success. Therefore, the number of thermograms were increased using data augmentation method.

In Fig. 14, when the 43 thermograms were used, the highest specificity rate was 100%, whereas this rate decreased to 98.28% when the 258 thermograms were used. Considering increases in the rates of sensitivity and accuracy, that tiny decrease in specificity rate can be ignored.

In conclusion, after the total image number was increased to 258 by applying data augmentation method, the higher classification success rate was reached.

## 5. Conclusion

In this study, a classification system based on multiresolution analysis methods to detect thermograms as healthy or unhealthy (with heart disease) was designed. Obtained results show that using multiresolution analysis methods to classify thermograms gave good results. These results indicate that a pre-diagnosis system which detects diseases early can be designed by combining multiresolution analysis and classification methods. Thus, the mortality rate in neonates can be reduced by detecting the disease using thermal imaging even under physical effects which do not indicate the disease. In conclusion, using thermal imaging and machine learning together will contribute to the medical field enormously.

Using thermal imaging to analyse physiological functions related to skin temperature of neonates and to construct temperature profiles is practical and easy. Thermal imaging is a non-invasive, un-ionic and non-contact method gaining importance to continuously track neonates who in neonatal intensive care units. Considering that the thermography which has recently been developed and started to use in biomedical field, it is clear that the success of the used method in this study can be improved using more dataset and advanced methods.

In future work, the classification system developed in this study will be applied to more various thermograms to achieve more objective results. In addition, different multiresolution analysis methods and different classification techniques will be used to evaluate classification successes. In this study, complex versions of multiresolution analysis methods were not used. Future studies will observe the effect of the use of complex versions on the success of the classification.

## Acknowledgements

This study was supported by the Scientific and Technological Research Council of Turkey (TUBITAK, project number: 215E019).

## References

[1] A. Rogalski, Chrzanowski K., “Infrared devices and techniques,” Opto-Electronics Review, vol. 10, no. 2, pp. 111–136, 2012.

[2] S. Sruthi, M. Sasikala, “A low cost thermal imaging system for medical diagnostic applications,” 2015 International Conference on Smart Technologies and Management for Computing, Communication, Controls, Energy and Materials (ICSTM), Chennai, India, pp. 621–623, 2015.

[3] C. Hildebrandt, K. Zeilberger, E. F. C Ring, C. Raschner, “The application of medical infrared thermography in sports medicine,” An International Perspective on Topics in Sports Medicine and Sports Injury, vol. 14, pp. 258–274, Feb. 2012.

[4] R. B. Knobel, B. D. Guenther, H. E. Rice, “Thermoregulation and thermography in neonatal physiology and disease,” Biological Research for Nursing, vol. 13, no. 3, pp. 274–282, 2011.

[5] B. F. Jones, “A reappraisal of the use of infrared thermal image analysis in medicine,” IEEE Transactions on Medical Imaging, vol. 17, no. 6, pp. 1019–1027, 1998.

[6] D. Savasci, A. H. Ornek, S. Ervural, M. Ceylan, M. Konak, H. Soylu, “Classification of Unhealthy and Healthy Neonates in Neonatal Intensive Care Units Using Medical Thermography Processing and Artificial Neural Network,” Classification Techniques for Medical Image Analysis and Computer Aided Diagnosis, Elsevier, 2019.

[7] A. H. Ornek, D. Savasci, S. Ervural, M. Ceylan, H. Soylu, “Termogramların Değerlendirilmesinde Doğru Yaklaşımların Belirlenmesi,” URSI-TÜRKİYE 2018 IX. Bilimsel Kongresi, KTO Karatay Üniversitesi, Konya, Turkey (in Turkish), 2018.

[8] O. Rioul, M. Vetterli, “Wavelets and signal processing,” IEEE Sig. Proc. Mag, pp. 14 – 38, Oct. 1991.

[9] S. AlZubi, N. İslam, M. Abbod, “Multiresolution analysis using wavelet, ridgelet, and curvelet transforms for medical image segmentation,” International Journal of Biomedical Imaging, no.4, pp. 1-18, 2011.

[10] M. Ceylan, “A new complex-valued intelligent system design on evaluating of the lung images with computerized tomography,” PhD, Selcuk University, Konya, Turkey (in Turkish with an abstract in English), 2009.

[11] M. N. Do, M. Vetterli, “The finite ridgelet transform for image representation,” IEEE Transactions on Image Processing, vol. 12, no. 1, pp. 16-28, March. 2003.

[12] J. M. Fadili, J. L. Starck, “Curvelets and ridgelets,” R.A. Meyers, ed. Encyclopedia of Complexity and Systems Science, 14, Springer New York, USA, 2009, pp. 1718-1738.

[13] E. Candes, L. Demanet, D. Donoho, L. Ying, “Fast discrete curvelet transforms,” Multiscale Modeling & Simulation, vo. 5, no. 3, pp.861-899, 2006.

[14] M. Ceylan, A. E. Canbilen, “Performance comparison of tetrolet transform and wavelet-based transforms for medical image denoising,” International Journal of Intelligent Systems and Applications in Engineering, vol. 5, no. 4, pp. 222-231, 2017.

[15] M. N. Do, M. Vetterli, “Contourlets,” In J. Stoeckler and G.V. Welland Editors, Beyond Wavelets, Academic Press 2002, pp. 1-27.

[16] G. H. Toro-Garay, R. J. Medina-Daza, “Fusion of WorldView2 images using contourlet, curvelet and ridgelet transforms for edge enhancement,” Revista Facultad de Ingeniería Universidad de Antioquia, Bogotá, Colombia, no. 85, pp. 8-17, Oct./Dec. 2017.

[17] M. N. Do, M. Vetterli, “The contourlet transform: an efficient directional multiresolution image representation,” IEEE Transactions on image processing, vol. 14, no. 12, pp. 2091-2106, Dec. 2005.

[18] F. Amato, A. López, E. M. Peña-Méndez, P. Vaňhara, A. Hampl, J. Havel, "Artificial neural networks in medical diagnosis," Journal of Applied Biomedicine, vol. 11, no. 2, pp. 47–58, 2013.

[19] I. Basheer, M. Hajmeer, "Artificial neural networks: Fundamentals, computing, design, and application" J Microbiol Meth, vol. 43, no. 3, pp. 3–31, Dec. 2000.

[20] M. Negnevitsky, "Artificial intelligence," A Guide to Intelligent Systems, Second Edition, 2005.

[21] J. A. Freeman, D. M. Skapura, "Neural networks algorithms, applications, and programming techniques," Computation and Neural Systems Series, Series Editor, 1991.

[22] C. Cortes, V. Vapnik, "Support-vector networks," Mach. Learn, vol. 20, no.3, pp. 273-297, 1995

[23] O. Chapelle, P. Haffner, and V. N. Vapnik, "Support vector machines for histogram-based image classification," IEEE transactions on Neural Networks, vol.10, no. 5, pp. 1055-1064, Sep. 1999.

[24] V. Vapnik, "The Nature of Statistical Learning Theory,"MJ New York: Springer-Verlag, vol.1, 1995.

[25] L. Breiman, "Random Forests," Machine learning, vol. 45, no. 1, pp. 5-32, Oct. 2001.

[26] L. Breiman, A. Cutler, "Random Forest" 2009, Online http://www.stat.berkeley.edu/~breiman/RandomForests/cc_home.htm

[27] K. J. Archer, "Emprical characterization of random forest variable importance measure, computational statistical data analysis," Computational Statistics & Data Analysis, vol. 52, no. 4, pp. 2249-2260, Jan. 2008.

[28] D. Sharma, U.B. Yadav, P. Sharma, "The concept of sensitivity and specificity in relation to two types of errors and its application in medical research" Journal of Reliability and Statistical Studies, vol. 2, no.2, pp. 53–58, 2009.

[29] D. Savasci, "Thermal Image Analysis for Neonatal Intensive Care Units," Master Thesis, Konya Technical University, Konya, Turkey (in Turkish with an abstract in English), 2019.